

Analysis of ductile Mixed-Mode I/II fracture initiation with a nonlinear CDM model

A. Pirondi¹ and N. Bonora²

¹ Department of Industrial Engineering, University of Parma, Parco Area delle Scienze 181/A, 43100 Parma, Italy

² Department of Industrial Engineering, University of Cassino, v. G. De Biasio 43, 03043 Cassino, Italy

***ABSTRACT:** in this study, boundary layer FE analyses of a mixed-mode I/II loaded crack are performed within the context of small-scale yielding conditions using the nonlinear CDM model developed in [1]. The model is implemented in the commercial FE code ABAQUS. The attention is focused on the modeling of incipient fracture and of the first steps of propagation.*

INTRODUCTION

The possibility to predict the failure of components under complex loading conditions is an attractive subject which led, in the last decades, to the development of constitutive models based on the so-called local approach. The many models can be grouped into two main categories: porosity models and Continuum Damage Mechanics (CDM) models.

Analyses of mixed-mode ductile fracture initiation have been made in the past using boundary layer FE model with the Gurson constitutive law [2-4]. In the Gurson model the porosity plays the role of a softening variable that progressively implodes the yield surface to account for damage.

In this study, boundary layer FE analyses of a mixed-mode I/II loaded crack are performed within the context of small-scale yielding conditions using the nonlinear CDM model developed in [1]. The model is implemented in the commercial FE code ABAQUS. The attention is focused on the modeling of incipient fracture and of the first steps of propagation.

NON-LINEAR CDM MODEL

The CDM models are developed in the framework of continuum mechanics and the damage effects are accounted for by a thermodynamic variable, D , [5]. Damage accounts for material progressive loss of load carrying capabil-

ity due to irreversible microstructural modifications, such as microvoids formation and growth, microcracking, etc. From a physical point of view, damage can be expressed as

$$D_{(n)} = 1 - \frac{A_{eff}^{(n)}}{A_0^{(n)}} \quad (1)$$

where, for a given normal n , $A_0^{(n)}$ is the nominal section area of the Representative Volume Element (RVE) which defines the mesoscale dimension, and $A_{eff}^{(n)}$ is the effective resisting one reduced by the presence of microflaws and their mutual interactions. If the damage is assumed to be isotropic, the scalar quantity D can be identified more easily as:

$$D = 1 - \frac{\tilde{E}}{E_0} \quad (2)$$

where E_0 and \tilde{E} are the Young's modulus of the undamaged and damaged material, respectively.

In [1] a new non-linear CDM model for ductile failure was proposed that was proven to match well the damage evolution for different classes of metals and to be effective in describing the decrease of ductility (*i.e.* strain to failure) with increasing stress triaxiality exhibited by ductile metals. This model was also successful in predicting the response of notched and cracked components using damage parameters identified by uniaxial tensile tests [6]. In this model, the damage dissipation potential f_D , similar in meaning to the one used for describing plasticity, has the following expression:

$$f_D = \left[\frac{1}{2} \left(-\frac{Y}{S_0} \right)^2 \cdot \frac{S_0}{1-D} \right] \cdot \frac{(D_{cr} - D)^{\frac{\alpha-1}{\alpha}}}{p^{\frac{2+n}{n}}} \quad (3)$$

where D_{cr} is the critical value of the damage variable for which ductile failure occurs, S_0 is a material constant and n is the material hardening exponent. The damage exponent α determines the shape of the damage evolution law and is related to the nature of the bond between brittle inclusions and the ductile matrix. The kinetic law of damage evolution is:

$$\dot{D} = -\dot{\lambda} \frac{\partial f_D}{\partial Y} = \alpha \cdot \frac{(D_{cr} - D_0)^{\frac{1}{\alpha}}}{\ln(\varepsilon_f / \varepsilon_{th})} \cdot f \left(\frac{\sigma_H}{\sigma_{eq}} \right) \cdot (D_{cr} - D)^{\frac{\alpha-1}{\alpha}} \cdot \frac{\dot{p}}{p} \quad (4)$$

A detailed description of the derivation of these equations can be found in

[1]. The function $f(\sigma_H/\sigma_{eq})$ that accounts for stress triaxiality effects in Eq. (4) is defined as:

$$f\left(\frac{\sigma_H}{\sigma_{eq}}\right) = \frac{2}{3}(1+\nu) + 3 \cdot (1-2\nu) \cdot \left(\frac{\sigma_H}{\sigma_{eq}}\right)^2 \quad (5)$$

that is derived assuming that ductile damage mechanism is governed by the total elastic strain energy, Lemaitre [5]. Here, $\sigma_H = \sigma_{kk}/3$ is the hydrostatic part of the stress tensor, σ_{eq} the von Mises equivalent stress and ν is the Poisson's ratio. The model requires five material parameters: the strain threshold (in uniaxial monotonic loading) ε_{th} , at which damage processes are activated; the strain ε_f at which failure occurs under uniaxial state of stress (i.e. $\sigma_H/\sigma_{eq}=1/3$); the initial amount of damage present in the material, D_0 ; the critical damage, D_{cr} , at which failure occurs and the damage exponent, α , that control the shape of damage evolution with plastic strain. The procedure for the identification of the damage parameters can be found in [6].

FINITE ELEMENT MODELING

A Boundary Layer technique is used in this study, that means only a circular portion of material around the crack tip is modeled. A slit with a round notch of radius $b_0/2$ at the end is introduced to simulate the presence of a crack. The mesh is composed of an outer portion centered on the tip with an angular discretization of 15° (Figure 1a) and an inner portion, with elements angularly spaced of 7.5° and a higher radial refinement (Figure 1b).

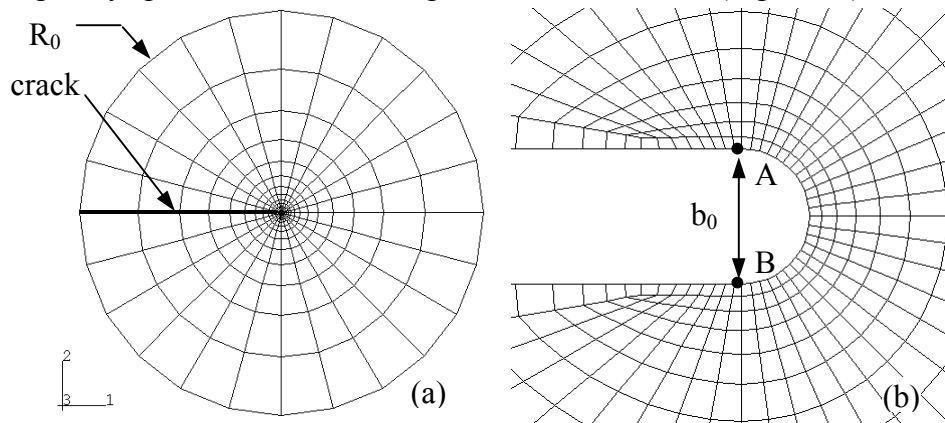


Figure 1: Outline of the FE model: (a) outer portion; (b) inner portion.

Four-noded isoparametric elements are used. The ratio between the notch and the outer radius is $(b_0/2)/R_0=10000$, so that plasticity is always well-contained within the boundary layer.

A finite strain formulation with incremental plasticity and associated von Mises flow rule was used in the simulations. Plane strain conditions were assumed. The material properties are that of SA 537 steel determined previously by one of the authors and are summarized in Table 1 ($D_0=0$).

TABLE 1: Material properties used in the simulations.

TENSILE PROPERTIES		DAMAGE PARAMETERS	
Young's mod., E (GPa)	190	D_{cr}	0.85
Poisson's ratio, ν	0.3	ϵ_{th}	0.0127
Yield stress, σ_0 (MPa)	380	ϵ_f	1.7
Hardening exponent, n	0.143	α	0.655

The mixed mode elastic K field is imposed on the outer boundary, that is:

$$u_1 = \frac{K_I}{2G} \sqrt{\frac{r_0}{2\pi}} \quad u_2 = \frac{K_{II}}{2G} \sqrt{\frac{r_0}{2\pi}} \quad (6)$$

Four values of the mixed mode elastic parameter $M_e=2/\pi*\arctan(K_I/K_{II})$ were simulated, namely $M_e=1$ (mode I), $M_e=0.667$, $M_e=0.333$ and $M_e=0$ (mode II).

RESULTS AND DISCUSSION

Preliminary analyses, restricted to mode I conditions, were devoted to study the sensitivity of the model to the element size and to the time increment of the solution. The sensitivity was defined on the basis of the value of K at the instant when the first group of elements failed at the crack tip. To vary the element size while keeping constant its shape, the notch radius and the radius of the inner portion of the model were changed accordingly. The results showed that the value of J at the instant of failure, J_i , increased with the element size but the corresponding value of $J_i/(\sigma_0 b_0)$ was almost constant. A different loading step within the range $0.25 \leq \Delta K \leq 2.5 \text{MPa}\sqrt{\text{m}}$ did not result in appreciable differences.

The first set of mixed mode analyses was limited at the instant when the first group of elements at the crack tip fails. In Figure 3 the contour plots of damage at the instant of failure are reported. Under mixed mode loading, the damage distribution is the result of the competition between the higher triaxiality at the blunted side of the tip and the strain concentration at the sharpened side. In fact, both factors affect the damage rate according to Eq. (10). Under mode I and mixed mode conditions, the influence of stress triaxiality is always prevailing and, therefore, the critical damage is attained at the blunted side of the tip. Under mode II loading, the strain concentration at the sharpened side is high enough to initiate a crack, although damage reaches a high value also at the blunted side.

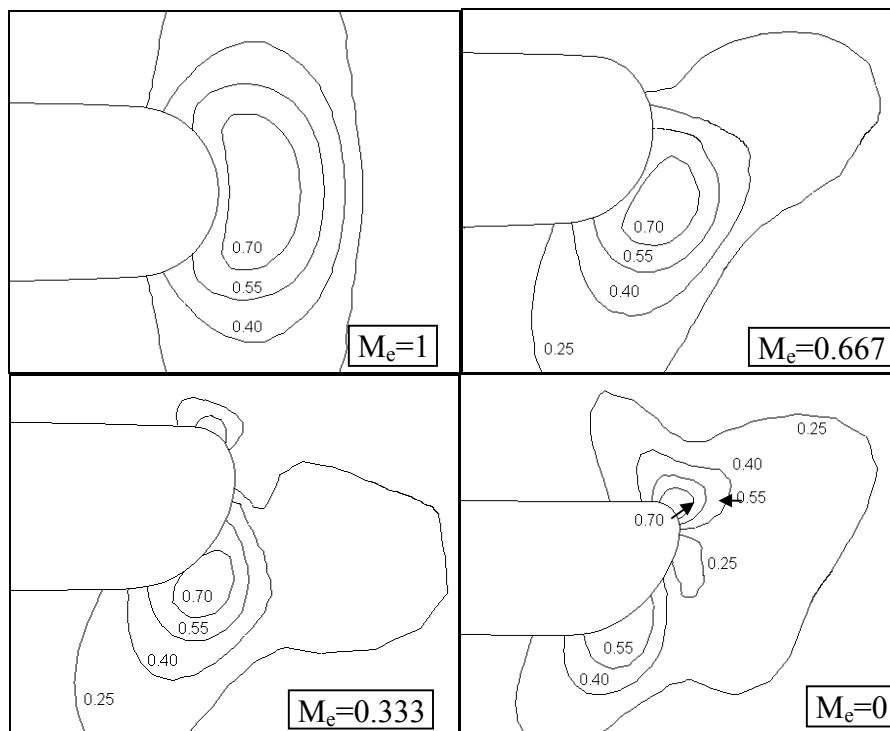


Figure 3: Contour plots of damage at the instant of failure.

In the mixed mode fracture envelope of Figure 4 the values of the mode I (K_I^i) and mode II (K_{II}^i) stress intensity factor at the instant of failure are reported, normalized with respect to the corresponding pure mode I value ($M_e=0$), $K_{I,i}$. Since the mixed mode fracture toughness of the SA 537 was not available, they have been compared with the mixed mode fracture envelopes predicted by the criteria [7-9]. The FE simulation results fall within

these criteria and are especially in good agreement with the maximum hoop stress theory [7], which predicts fracture to occur along the plane of maximum hoop stress at the crack tip.

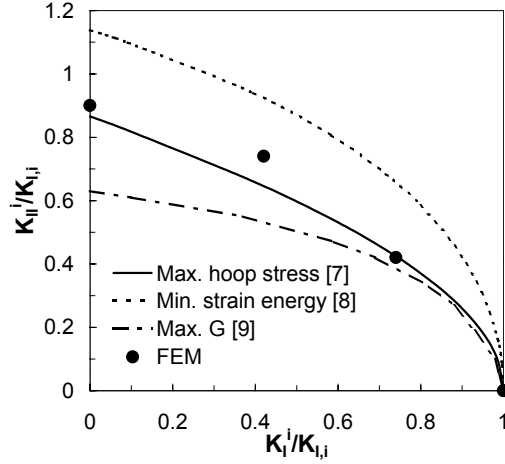


Figure 4: fracture envelope predicted by FEM and by [7-9].

The first steps of crack propagation are shown in Figure 5. The crack always kinks towards the blunted side with the exception of Mode II loading, where it branches at both the blunted and sharpened sides. As the branched cracks progress, the one at the sharpened side closes up, eventually arresting the crack advance. Unfortunately, this kind of varying self-contact conditions are very difficult to implement in the simulation, therefore the propagation of this branch of the crack may be fictitious. Also from the physical standpoint the propagation at the sharpened side should be delayed, because a highly negative triaxiality, such as the one that develops there, increases material ductility [10]. In the case of homogenous, low-hardening metals, an almost co-planar crack advance is often observed under Mode II loading [11-13] but, in this case, the underlying mechanism is a void-sheeting [14] rather than void nucleation, growth and coalescence. In short, damage should not be modeled in the same way for positive and for negative triaxiality, as discussed in [15]. If we assume, as in [15], that the damage rate is zero for negative triaxiality, the Mode II loaded crack can only propagate at the blunted side.

The angle θ_i between the initial and the kinked crack, measured on the undeformed configuration, is reported in Figure 6 as a function of M_e along with the fracture criteria [7-9]. The angle increases with increasing mode II loading as it is generally observed experimentally. The FE results lie

slightly below the fracture criteria but are again not far from the maximum hoop stress criterion. The radial and angular discretization probably play a role in determining this difference.

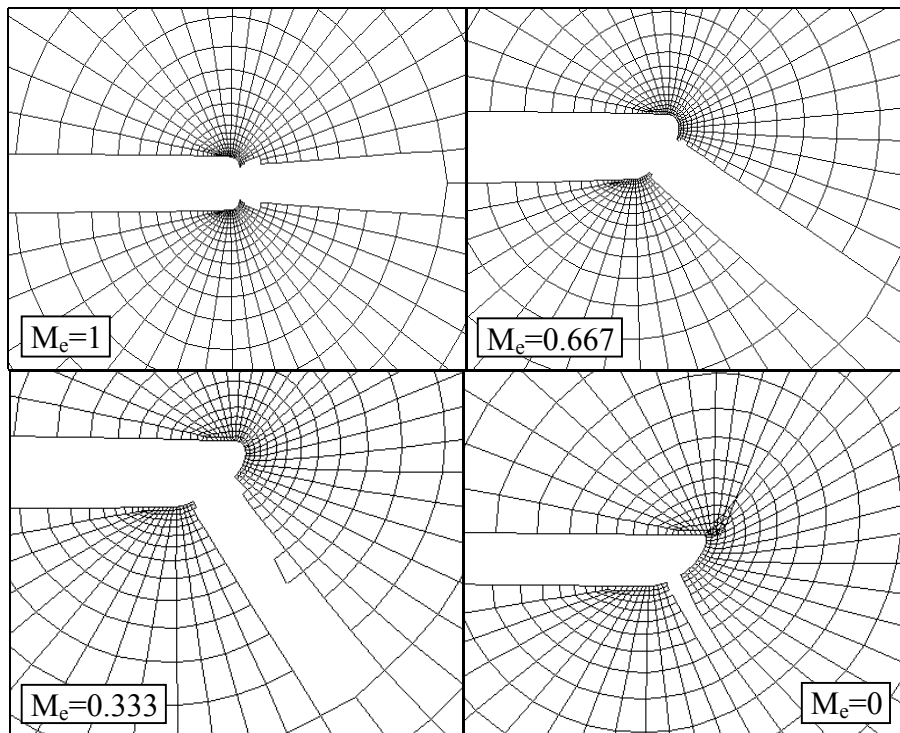


Figure 5: First steps of crack propagation.

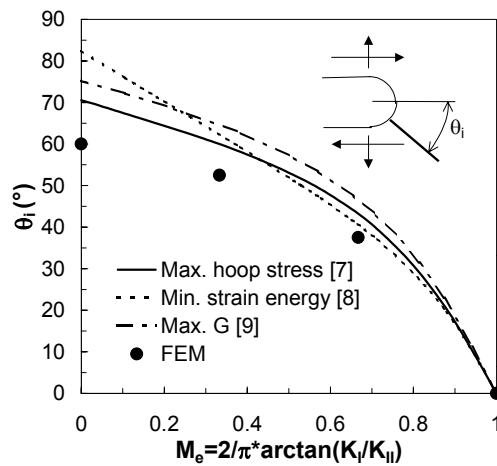


Figure 6: crack initiation angle predicted by FEM and by [7-9].

CONCLUSIONS

A FE analyses of a mixed-mode I/II loaded crack was performed using a boundary layer technique. Material damage was introduced using the non-linear CDM model developed in [1]. The mixed-mode fracture envelope predicted by the model is in good agreement with the maximum hoop stress criterion. The CDM-predicted crack initiation angle instead lies slightly below that criterion.

REFERENCES

1. Bonora, N. (1997) *Engineering Fracture Mechanics*, **58**, 1/2, 11-28.
2. Aoki, S., Kishimoto, K., Yoshida, T., Sakata, M. (1987) *Journal of the Mechanics and Physics of Solids*, **35**, 4, 431-455.
3. Ghosal, A.K., Narasimhan, R. (1994) *Journal of the Mechanics and Physics of Solids*, **42**, 6, 953-978.
4. Ghosal, A.K., Narashiman, R. (1996) *Materials Science and Engineering*, A211, 117-127.
5. Lemaitre, J. (1985) *Journal of Engineering Materials Technology*, **107**, 83-89.
6. Bonora, N. (1999) *Journal of Strain Analysis*, **34**, 6, 463-478.
7. Erdogan, F., Sih, G.C. (1963) *Journal of Basic Engineering*, 85, 519-525.
8. Sih, G.C. (1974) *International Journal of Fracture*, 10, 305-321.
9. Hussain, M.A., Pu, S.L., Underwood, J. (1974). In: *ASTM STP 560*, pp. 2-28, American society for Testing and Materials, Philadelphia, USA.
10. Pugh, H.L.D. (1970), *The mechanical behaviour of materials under pressure*, Elsevier Publ. Co., Barking, UK.
11. Davenport, J.C.W., Smith, D.J. (1994). In: *ECF 10*, Schwalbe K.-H., Berger C., eds. EMAS, pp. 901-910.
12. Bhattacharjee, D., Knott, J.F. (1994) *Acta metallurgica et materialia*, **42**, 5, 1747-1754.
13. Pirondi, A., Dalle Donne, C. (2001) *Engineering Fracture Mechanics*, **68**, 12, 1385-1402.
14. Beachem, C.D. (1975) *Metallurgical Transactions A*, 6A, 377-383.
15. Pirondi, A., Bonora, N. (2001) *Computational Materials Science*, to appear.